scientific reports

Check for updates

OPEN

Interface modes in planar one-dimensional magnonic crystals

Szymon Mieszczak✉ & Jarosław W. Kłos

We present the concept of Zak phase for spin waves in planar magnonic crystals and discuss the existence condition of interface modes localized on the boundary between two magnonic crystals with centrosymmetric unit cells. Using the symmetry criterion and analyzing the logarithmic derivative of the Bloch function, we study the interface modes and demonstrate the bulk-to-edge correspondence. Our theoretical results are verified numerically and extended to the case in which one of the magnonic crystals has a non-centrosymmetric unit cells. We show that by shifting the unit cell, the interface modes can traverse between the band gap edges. Our work also investigate the role of the dipolar interaction, by comparison the systems both with exchange interaction only and combined dipolar-exchange interactions.

Band structure is a distinctive feature of wave excitations in periodic structures. Solutions of the wave equations in a periodic medium, Bloch waves are characterized by the quasimomentum $\hbar\boldsymbol{k}$, related to the wavevector $\boldsymbol{k}$. Adiabatic changes of the wavevector in the momentum space lead to the acquisition of a geometrical phase. Introduced by M. Berry[1], this phase is related to the topological invariants that distinguish the topological classes of the system. For Bloch waves $\Phi_k(x)$ propagating in a periodic 2D or 3D medium this role is played by Chern numbers[2–4], which are determined for successive bands from the Berry phases calculated along a closed loop in the momentum space - i.e., along the edge of 1st Brillouin zone. In a 1D system a loop for the Berry phase can be realized by sweeping the wavenumber k across the 1st Brillouin zone (i.e., in the range $[-\pi/a, \pi/a]$, where a is the period of the structure). Then, we take advantage of the periodicity of the Bloch function in the reciprocal space: $\Phi_k(x) = \Phi_{k+2\pi/a}(x)$. Referred to as the Zak phase[5,6], this phase characterizes each band of a 1D crystal due to the lack of degeneration in 1D systems. The Zak phase can be altered by changing other parameters of the system (e.g., by tuning its structural and material parameters) significantly enough to disturb the band structure resulting in band gap closing and reopening.

The Zak phase has an ambiguity related to the selection of the unit cell[7]. However, for a centrosymmetric unit cell it only takes on two well-defined values, which are 0 and π. These values classify the bands in two categories and distinguish the types of band gaps[6,8,9]. The classification can be based on the symmetry of the Bloch functions on the edges of the bands/gaps[8,10]. This can help establish the criteria for the existence of edge or interface modes[8] in terminated periodic structures, where bulk characteristics (symmetry of the bands and their Zak phases) correlate with surface parameters determining the existence of edge modes in the band gaps.

Zak phase and edge modes have been the subject of investigation in 1D continuous systems in the form of layered media or periodically corrugated waveguides. Various kinds of systems have been studied, including photonic crystals[11,12], microwave systems[13,14], plasmonic crystals[15] and phononic crystals[16]. It is worthy of notice that the definition and interpretation of surface parameters can vary with system. Examples include the rate of decay of electron waves outside the crystal (e.g., in vacuum[8]), surface impedance for electromagnetic waves[12], or pinning parameter for spin waves[17]. The Zak phase is measurable quantity[7] and is a powerful tool to predict the existence and to describe properties of surface/edge modes.

The studies on spin waves in magnonic crystals[18–20] reported to date, mostly address lattice models based on the Heisenberg Hamiltonian[21–23] or the Landau-Lifshitz equation, but discretized in the second-quantization approach to the Bogliubov-de Gennes Hamiltonian[24]. They strongly indicate the importance of the Dzyaloshinskii-Moriya interaction and dipolar interaction for the occurrence of non-zero Chern numbers. A general discussion of the topological origin of magnetostatic surface spin waves has been provided recently in Refs.[25–27]. Topological concepts can be used to reinterpret those studies of spin-wave defect and edge states in magnonic crystals[28–34] which discuss the existence of localized states in terms of symmetry criteria[8].

In this paper we demonstrate that (i) the same standard formula for the Zak phase as used for electronic states[1] applies to both exchange and exchange-dipolar spin waves in 1D planar magnonic crystals; (ii) in magnonic crystals with centrosymmetric unit cell the Zak phase can be determined by a symmetry-related criterion, and

Institute of Spintronics and Quantum Information, Faculty of Physics, Adam Mickiewicz University, Poznań, Poland. ✉email: szymon.mieszczak@amu.edu.pl
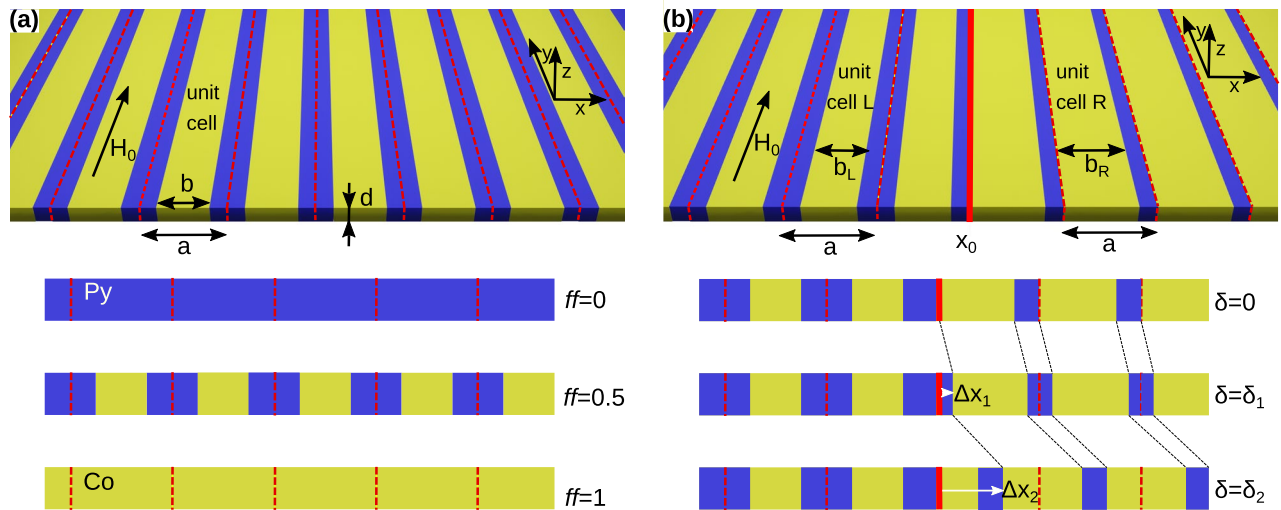
Figure 1. (**a**) The geometry of the one-dimensional magnonic crystal. Red dashed lines mark the edges of centrosymmetric unit cells of the size a (lattice constant). Yellow and blue colors distinguish the strips made of Co and Py of the width: b and $a - b$, respectively. The strips are thin $d \ll a$, and the magnetic field H_0 is applied along the strips (static demagnetizing effects are absent). In our studies, we changed the width of both strips, keeping the lattice constant fixed (see the inset below **a**). By sweeping the bulk parameter (i.e., the filling fraction) $ff = b/a$ in the range $[0, 1)$, we can tune the SW spectrum between the limits corresponding to the uniform layer of Py ($ff = 0$) and Co ($ff = 1$). (**b**) Two semi-infinite magnonic crystals differing in filling fractions ($ff_L \neq ff_R$), interfaced at the edges of units cells (solid red line). For the magnonic crystal on the left (right) side, we chose a centrosymmetric (non-centrosymmetric) unit cell. The selection of the unit cell does not affect the spectrum of the infinite magnonic crystal but is important for the formation of interface states. The parameter $\delta = \Delta x / a = [0, 1)$, describing the selection (i.e., the shift) of the unit cell, can then be treated as an interface parameter (see the inset below **b**). The values δ_1, δ_2 (and Δx_1, Δx_2) correspond to two possible selections of centrosymmetric unit cell.

the values of the Zak phase for successive bands can be used to investigate the existence of interface states on the boundary between two semi-infinite magnonic crystals; (iii) the calculations done for the fictitious model, where the dipolar interactions were switched off, shows a close analogy to the electronic system; (iv) the numerical calculations performed for a realistic, dipolar-exchange system confirm the theoretical predictions regarding the existence of interface spin-wave modes.

Structure and model

Structure. We investigate the spin-waves (SWs) localized on the interface between two one-dimensional magnonic crystals (1D MCs). Each 1D MC is built from two kinds of strips, differing in magnetic parameters, that are arranged periodically in the plane, being in direct contact with each other. The structure of a single 1D MC is schematically presented in Fig. 1a. Such a system can be fabricated by lithographic techniques[35–37], where two different materials can be deposited in separate areas, by the ion implantation, where magnetic anisotropy, magnetization saturation, or exchange length can be changed in initially homogeneous magnetic layer[38,39], or by inducing a thermal gradient that suppress locally the magnetization saturation[40]. In our model, we consider two sets of parameters corresponding to widely used materials, namely cobalt (Co) and permalloy (Py). The properties that are important for SW propagation are saturation magnetization M_S and exchange length λ_{ex}. These parameters are equal to $M_{S,Co} = 1445$ kA/m, $\lambda_{ex,Co} = 4.78$ nm, $M_{S,Py} = 860$ kA/m, $\lambda_{ex,Co} = 5.29$ nm. We assumed that both materials are amorphous, and there is no magnetocrystalline or surface magnetic anisotropy in our system. The strips are flat, i.e., their thickness d is much smaller than their width. This assumption allows restricting our consideration to the SW fundamental mode, that is not quantized across the thickness. Additionally, we assume that our sample is saturated by an external magnetic field of the magnitude $\mu_0 H_0 = 0.2$ T oriented along the strips. For this magnetic configuration, the static demagnetizing field is equal to zero.

Two semi-infinite 1D MCs are jointed as it is presented in Fig. 1b. They are interfaced on the edges of their unit cells. The strips in both MCs are made of the same materials (Py and Co), and have the same period a and thickness d. The structures on both sides of the interface differ only by: (i) the filling fractions ff—the ratio between the width of Co strip b and the period a ($ff = b/a$) and (ii) the selection of the unit cell—described by the parameter δ. In the 1D crystal, the unit cell of the width a can be shifted by arbitrary distance in the range $\Delta x = [0, a)$ ($\Delta x = 0$ denotes unit cell with the whole Co(Py) strip on the left(right) side of unit cell). This selection does not affect the spectrum of infinite crystal (i.e., the band structure of propagating modes) but is important for the existence of surface/interface modes in the structures terminated at the edge of the unit cell. The parameter $\delta = \Delta x / a$ has two distinguished values equal to: $\delta_1 = 1/2 - ff/2$, $\delta_2 = 1 - ff/2$. For these values unit cell becomes centrosymmetric. We calculated the Zak phase and logarithmic derivative of Bloch function for δ_1, where both 1D MCs have the same type of symmetry, i.e., Co strip is placed in the middle of the unit cell.

Please also note that the cells for $\delta = 0$ and $\delta = 1$ are equivalent. In our studies, we are investigating the existence of SW modes localized on the interface between two 1D MC in the function of bulk parameter ff and interface parameter δ. One can imagine the system design based on modulation of some other bulk parameter, like value of external magnetic field[41,42], thickness modulation[43–45], or interface/surface parameters, like the modifications of the structures close to the interface/surface[29,31].

Model for magnetization dynamics.   We describe the SW modes in 1D MCs using the classical approach, based on the Landau-Lifshitz equation (LLE), which is an equation of motion for spatially dependent magnetization vector $\boldsymbol{M}(\boldsymbol{r}, t)$ in the effective magnetic field $\boldsymbol{H}_{\text{eff}}(\boldsymbol{r}, t)$:

$$\partial_t \boldsymbol{M} = -\mu_0 |\gamma| \boldsymbol{M} \times \boldsymbol{H}_{\text{eff}}, \tag{1}$$

where $\mu_0 = 4\pi \times 10^{-7} \text{H/m}$ is the permeability of vacuum and $|\gamma| = 194.6 \text{ GHz/T}$ gyromagnetic ratio. In our case $\boldsymbol{H}_{\text{eff}}$ is composed of the following terms:

$$\boldsymbol{H}_{\text{eff}}(\boldsymbol{r}, t) = \boldsymbol{H}_0(\boldsymbol{r}) + \boldsymbol{H}_{\text{dm}}(\boldsymbol{r}, t) + \boldsymbol{H}_{\text{ex}}(\boldsymbol{r}, t). \tag{2}$$

The symbols: $\boldsymbol{H}_0$, $\boldsymbol{H}_{\text{dm}}(\boldsymbol{r}, t)$ and $\boldsymbol{H}_{\text{ex}}(\boldsymbol{r}, t)$ stand for external field, demagnetizing field and exchange field, respectively. The last two terms are both spatially and temporally dependent since they are related to dynamic exchange and dynamic dipolar interaction. The SWs are calculated in linear approximation, where the magnetization dynamics can be considered as precession motion around the static magnetic configuration $\boldsymbol{M}(\boldsymbol{r}) \approx M_S \hat{\boldsymbol{y}}$ with dynamic component $\boldsymbol{m}(\boldsymbol{r}, t) = \boldsymbol{m}(\boldsymbol{r}) e^{i\omega t}$ circulating harmonically in time, with the frequency ω: $\boldsymbol{M}(\boldsymbol{r}, t) = \boldsymbol{M}(\boldsymbol{r}) + \boldsymbol{m}(\boldsymbol{r}) e^{i\omega t}$. We consider only the case where SWs propagate along the direction of periodicity $\hat{\boldsymbol{x}}$. Therefore, the SW amplitude $\boldsymbol{m}(x) = m_\parallel(x) \hat{\boldsymbol{x}} + m_\perp(x) \hat{\boldsymbol{z}}$ depends only on $x-$coordinate only. In linear approximation the LLE (1) has a form of the set of two ordinary linear differential equations with periodic coefficients (see Supplementary Information, Section 1). Therefore, according to the Floquet's theorem[46], their solutions can be presented as Bloch function $\boldsymbol{m}_k(x) = \boldsymbol{u}_k(x) e^{ikx}$ with two complex components $m_{k,\parallel}, m_{k,\perp}$ related to in-plane and out-of plane magnetization dynamics, respectively. The symbol k stands for the wavenumber and $\boldsymbol{u}_k(x) = u_{k,\parallel}(x) \hat{\boldsymbol{x}} + u_{k,\perp}(x) \hat{\boldsymbol{z}}$ is periodic component of the Bloch function: $\boldsymbol{u}_k(x) = \boldsymbol{u}_k(x + a)$.

In this study, we consider SW spectra for two kind of effective field: (i) dipolar interaction are neglected; (ii) dipolar interactions are included. In the first case, we assumed that the unit cell has a size equal to $a = 100$ nm, while in the second, $a = 1000$ nm. In both cases, the thickness $d = 20 \text{ nm} \ll a$ and in the model, we assume an infinite length of strips that gives us an effectively 1D system.

Interface states.   We followed the work[6] to determinate the Zak phase as a topological characteristic of every (nth) band of the dispersion relation:

$$\theta_n = \Im \int_{-\pi/a}^{\pi/a} \frac{\int_{-a/2}^{a/2} \boldsymbol{u}_{n,k}^* \cdot \partial_k \boldsymbol{u}_{n,k} dx}{\int_{-a/2}^{a/2} \boldsymbol{u}_{n,k}^* \cdot \boldsymbol{u}_{n,k} dx} dk, \tag{3}$$

for two 1D MCs which were then joined at the common interface. In supplementary Information, Section 1, we present a detailed discussion of the applicability of the formula (3) to SW. The value of the Zak phase depends on the selection of the unit cell[7]. For the centrosymmetric unit cell, the Zak phase takes two quantized values, either 0 or π and can be deduced from symmetry criterion of modes (see Supplementary Information, Section 2 for details).

The necessary condition to observe the SW modes localized on the interface of two 1D MCs (Fig. 1b) is an overlapping some frequency gaps in the spectra of both 1D MCs. This fact ensures the exponential decaying of the mode on both sides of the interface, with the rate $\pm k_i$. For centrosymmetric unit cell, the logarithmic derivative is real and has a constant sign within the gap[8] (see Supplementary Information, Section 2). Therefore, the matching of the signs of logarithmic derivatives of Bloch function:

$$\rho(k) = \left. \partial_x \ln \left(m_{k,\alpha}(x) \right) \right|_{x=x_{0\pm}} = \left. \frac{\partial_x m_{k,\alpha}(x)}{m_{k,\alpha}(x)} \right|_{x=x_{0\pm}}, \tag{4}$$

on both sides of the interface between two 1D MCs ($x = x_{0\pm}$) is equivalent to the fulfillment the boundary conditions for $m_{k,\alpha}$ (for each component ($\alpha = \{\perp, \parallel\}$). These conditions allow finding the SW interface modes. It is worth noting that that we can limit our consideration only to one complex component of the Bloch function because $m_{k,\perp}/m_{k,\parallel} = C e^{-i\pi/2}$, where C is real and has a constant sign, determined by the direction of precession ($C = 1$ for purely exchange waves).

The relation between the sign of logarithmic derivative ρ in the gap above nth band and Zak phases θ_m can be written for 1D MC of centrosymmetric unit cells as[12] (see Supplementary Information, Section 2):

$$\text{sgn}(\rho) = \pm (-1)^{n-1} \exp \sum_{m=1}^{n} i\theta_m, \tag{5}$$

where $m = 1, \ldots, n$ indexes all bands below the gap. The signs '+' and '-' in the formula (5) refers to two possible selection of the complex wavevector in the gap, which describes the mode decaying to the right ($k = k_r + ik_i$) and to the left ($k = k_r - ik_i$) in the crystal, respectively[10] ($k_i > 0$). The Eq. (5) relates the topological parameter (Zak phases) characterizing the bands of 1D MC(s) with the boundary condition at the interface (expressed by

the logarithmic derivative of the SW amplitude). The modes localized on the interface between two 1D MCs can (cannot) exist when the signs of logarithmic derivative are the same (different) on both side of the interface (see the plots of ρ for both 1D MC in Supplementary Information, Section 2). It means that the expression $(-1)^{n-1} \exp \sum_{m=1}^{n} i\theta_n$ must have opposite signs on both side of the interface to compensate the change of the sign related to different direction of decaying of interface modes for $x \to \pm\infty$ (i.e., the signs '±' at the beginning of the formula for $\mathrm{sgn}(\rho)$ - see Supplementary Information, Section 2 for details).

The logarithmic derivative taken at the symmetry points of centrosymmetric unit cells has zeros and poles only at the edges of frequency gaps and ρ is real inside the gaps (see Supplementary Information, Section 2). It means that ρ cannot change its sign inside the gap. Therefore, the agreement of the signs of ρ in common frequency gaps, and eventually the existence of interface modes, depends on qualitative features of both 1D MCs spectra. More precisely, depends on the sequences of zeros and poles of ρ at gaps/bands boundaries and its signs in successive gaps. We show in the Supplementary Information, Section 2 that mentioned qualitative changes in the spectrum can be expresses as a $0 \leftrightarrow \pi$ flips of Zak phase θ.

It is worth noting that there are always two ways to select the centrosymmetric unit cell (i.e., there are two symmetry centers shifted by half of the period $\Delta x = a/2$) which are not equivalent for ρ and θ. When we shift the centrosymmetric unit cell by $a/2$ then θ flips $0 \leftrightarrow \pi$ in every band and ρ is negated in every second gap (see the Supplementary Information, Section 2 for explanations).

The more general case is when the unit cells are not selected as centrosymmetric. Then, the symmetry-related criteria for the existence of interface modes cannot be used. However, we can test the continuous transition between two different centrosymmetric selections of the unit cell. We investigate numerically how the shift of the unit cell Δx, described by the parameter $\delta = \Delta x/a$, influences the existence of SW interface modes. We will keep the centrosymmetric unit cell for the 1D MC on the left side (see Fig. 1b) and change the selection of the unit cell for 1D MC on the right by swapping the parameter δ in the whole range $[0, 1)$. For the gradual change of δ, we should observe the continuous transition of the frequencies of the SW interface modes between the boundaries of the gap. The SW interface modes for the values δ_1 and δ_2 correspond to the selection of centrosymmetric cell for the 1D MC on the right side of the interface. In this case, the observation of interface states must be consistent with the symmetry-related existence conditions for these states.

Numerical calculations. The LLE is solved by Plane Wave Method (PWM), which is suitable for periodic structures. Detailed discussion of the application of this computational method for planar magnonic crystals is presented in the paper by Krawczyk et al.[47]. Solving LLE with PWM gives us the information of dispersion relation and SW's eigenmodes. The bulk properties of SW in single unit cell (infinite 1D MC) are investigated for the one-dimensional unit cell with periodic boundary conditions. The calculations are done independence on the bulk parameter: filling fraction (ff).

To calculate the SW interface modes, we use a supercell approach[48]. We mimic two semi-infinite 1D MC, joined at the interface, by the supercell composed by finite 1D MC of two kinds, each consisting of $N = 100$ unit cells. Inevitable artifact of this approach is existence of second (complementary) interface, due to periodic boundary conditions, which can also bound the SW interface modes. Therefore, in our calculation, we will see two modes localized on different interfaces. This modes will be degenerated (and will occupy both interfaces at the same frequency) for $\delta = \delta_1$ or $\delta = \delta_2$, where unit cells are centrosymmetric and both interfaces are structurally identical.

For the geometry presented in Fig. 1b, the number of unit cells within each 1D MC should diverge to infinity. However, due to computational power limitations, we are constantly forced to perform the computations on the finite domain. To reproduce the spectrum of SW interface modes satisfactorily, we must consider the large supercell, where the distance between two interfaces is enough to avoid overlapping decaying exponentially "tails" of interface modes. For considered structures, this condition is fulfilled even for the smallest gap (characterized by small decay rates k_i) when taking about 100 unit cells of each MCs. Thus the length of each 1D MC is $D = Na$, where N is the number of unit cells and a unit cell's width. Such systems can be easily investigated on a desktop computers.

Results

Firstly, we consider the fictitious planar 1D MC with neglected dipolar interaction. This step allows us later to isolate the impact of dipolar interaction on the existence conditions of interface modes. We assumed a small lattice constant, $a = 100$ nm, where dipolar interaction would be negligible anyway. Nevertheless it is important to note, that even for small unit cell, system with dipolar interaction would vary in the following aspect: (i) dispersion relation is shifted up; (ii) dispersion relation is dependent on the direction of the external magnetic field; (iii) for k close to 0 group velocity is nonzero; (iv) for k close to 0 precession of magnetization vector is not perfectly circular.

Secondly, we consider the planar 1D MC with included dipolar interaction. To make them meaningful and propose a structure that is accessible experimentally, we assumed lattice constant, $a = 1000$ nm. In Supplementary Information, we show that the Zak phase for dipolar-exchange system (i.e., the system where the elliptical precession must be taken into account) is defined in the same way as for exchange systems. Therefore, the calculation of the Zak phase and logarithmic derivative can be performed in the same manner.

Exchange spin waves. For the system of the small lattice constant $a = 100$ nm, we neglected the dipolar interactions. We start the discussion by analyzing the dependence of the band structure of infinite MC on the bulk parameter—ff. In Fig. 2, the gray and white areas mark the frequency bands and gaps, respectively. For exchange spin waves, the gaps in 1D MC are opened alternatively in the center of the 1st Brillouin zone (BZ),
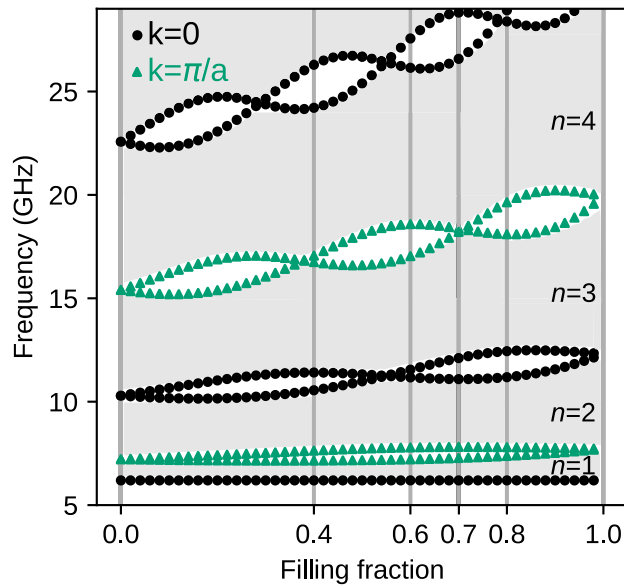
Figure 2. The evolution of SW spectra in dependence of the bulk parameter: filling fraction ff for exchange dominated 1D MC ($a = 100$ nm). White areas represents frequency gaps, while gray regions correspond to the successive frequency bands: $n = 1, 2, 3 \dots$. The edges of the bands: $k = 0$ and $k = \pi/a$ are marked by black dots and green triangles, respectively. The vertical lines at $ff = 0.4, 0.7$ and $ff = 0.6, 0.8$ denote the pairs which were interfaced to look for the SW interface modes in common frequency gaps.

i.e., for $k = 0$, and edge of the 1st BZ, i.e., for $k = \pi/a$ (see also Fig.3). These values determine the edges of gaps: black dotted line for $k = 0$ and green dotted line for $k = \pi/a$. In the absence of magnetocrystalline anisotropy, the lowest black line is independent of the material or structural parameters, including ff. Its position reflects the Larmor frequency and is determined only by the external magnetic field. The edges of higher gaps (i.e., located above successive bands $n = 1, 2, 3, \dots$.) are interwoven and cross each other at specific values of filling fraction ff (see also Fig.3(b)). The values of ff at which the gaps are closed correspond to the cases when both the Co and Py layer contains the integer number of the half-wavelengths. It is equivalent to the appearance of standing SWs. The resulting fact is that SW does not scatter on Co|Py interfaces for this particular frequency. It is worth noting that for $ff = 0$ or 1, the system is composed of homogeneous Py or Co where the periodicity and the folding of dispersion relation are introduced artificially. The points at which the folded dispersion self-crosses, mark the frequencies for which the (Bragg) gaps start to open when we introduce thin layers of other material. For $ff \approx 0$ (for Py matrix with thin Co layer), the gaps are opened at smaller frequencies than the corresponding gaps for $ff \approx 1$. Co has larger exchange length of Co, so the slope of its (parabolic) dispersion relation increases faster with the wavenumber and the sections of dispersion relations (bands) folded into the 1st BZ are wider in frequency domain. Therefore, the gaps not only interwove their edge with increasing ff but also push towards higher frequencies. Relatively narrow band gaps make designing the magnonic system with neglected dipolar interactions difficult, and proper selection of the system's properties become crucial.

Due to the reversing of the order of the gap's edges, the Zak phases (3) of two surrounding bands are flipped, and the sign of logarithmic derivative (4) inside the gap is negated. This observation concludes that by adjusting the bulk parameters (i.e., filling fractions ff) for two 1D MCs joined at the interface, we can adjust the topological parameters of their spectra to obtain a common frequency gap. The matching of boundary conditions expressed by agreement of logarithmic derivatives of the Bloch functions, exponentially decaying in the interior of corresponding 1D MC, can be achieved (see Supplementary Information, Section 2).

In the numerical studies of interface modes, we will also investigate the more general case, when the unit cell for one 1D MC is not centrosymmetric and thus it is not interfaced with other 1D MC at its symmetry point.

Interface modes for $ff_L = 0.4$ and $ff_R = 0.7$. Figure 3a–c presents the dispersion relation within the 1st BZ for three selected filling fractions $ff = 0.4, 0.54, 0.7$. The dispersion branches in Fig. 3a–c are labeled with Zak phase, as well as edges of band gaps with the value of the logarithmic derivative ρ (see Supplementary Information, Section 2)—the marked values are valid for centrosymmetric unit cell, where $\delta = \delta_1$. For the value $ff \approx 0.54$ (Fig.3b), we observe the crossing of second ($n = 2$) and third ($n = 3$) band and closing the gap between these bands. Due to the band crossing, the Zak phases for $n = 2$ and $n = 3$ are flipped, where the change of the symmetry of the Bloch mode at the bands' edges are related to the change of Zak phase (modes profiles are presented in Supplementary Information, Section 4). Now, when we join two semi-infinite MCs of the filling fractions (with centrosymmetric unit cell: $\delta = \delta_1$) $ff_L = 0.4 < 0.54$ and $ff_R = 0.7 > 0.54$ (Fig. 3a, c), then we can agree with the sign of the logarithmic derivatives of Bloch function on both sides of the interface in the common frequency gap (see Supplementary Information, Section 3). Please note that, for the same sequence of the Zak phases for
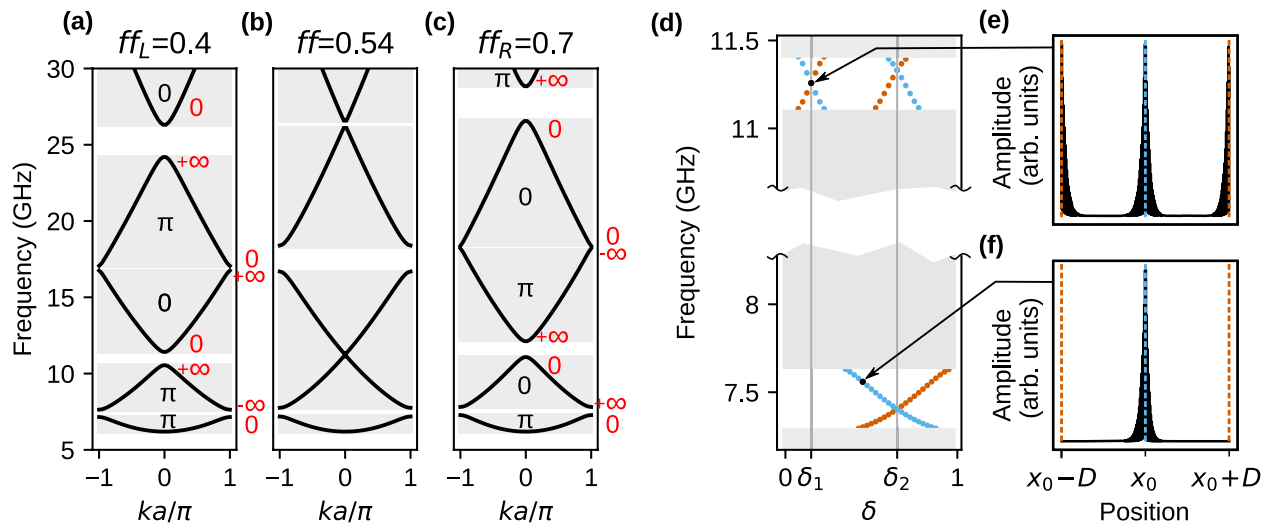
Figure 3. (**a–c**) Closing and reopening of the frequency gap (above the 2nd band, in the center of 1st Brillouin zone: $k = 0$) with the changes of filling fraction ff for exchange waves. The successive dispersion relations were plotted when the gap is (**a**) opened, $ff_L = 0.4$, (**b**) just closed, $ff = 0.54$, and (**c**) opened again, $ff_R = 0.7$. The labels: 0 and π stand for the Zak phases of the bands, 0 and ∞ (red color) - for logarithmic derivative on the edges of band gaps. The values of Zak phases and logarithmic derivatives were determined for the case $\delta = \delta_1$ (i.e., for Co strip in the center of the unit cell). The SW interface modes localized on the interface of two 1D MCs of $ff_L = 0.4$ and $ff_R = 0.7$. (**d**) The spectrum in the function of the surface parameter δ, defining the selection of the unit cells for 1D MC on the right. The values δ_1 and δ_2 correspond to the centrosymmetric unit cell with Co and Py strip in the middle. The calculations were performed for supercell approximation, where we considered the final sections of the 1D MCs, each of the size $D = Na$ and composed of $N = 100$ unit cells. Due to the application of periodic boundary conditions, we obtain an additional interface between 1D MCs. The frequency of interface mode localized in the center $x = x_0$ (on edge $x = x_0 \pm D$) of a supercell is marked by a blue dotted (orange dotted) line. (**e**, **f**) The profiles of the SW interface modes in the gaps above 1st and 2nd bands. The frequency and δ positions, for which modes are calculated, are indicated by arrows. The interfaces $x = x_0$ and $x = x_0 \pm D$ are pointed by blue dashed and orange dashed lines, respectively. For centrosymmetric case, the mode occupy both interface (e), while for non-centrosymmetric only one (**f**).

successive bands, the signs of logarithmic derivatives of Bloch functions decaying to the left or right (i.e., for the left and right 1D MC, respectively) are opposite in corresponding gaps (i.e., in the gaps between the same bands). Therefore, the band crossing is required to negate the sign of logarithmic derivatives $\text{sign}(\rho)$ in the reopened gap between the crossed bands (see the Supplementary Information 2 and 3 for more explanations) and ensure the matching of ρ on both sides of the interface.

Let us confirm the existence of interface states directly. For the two jointed semi-infinite 1D MCs (system presented in Fig. 1b), we ran PWM calculation (using the supercell approach) and collected SW spectra for wavenumber $k = 0$ (i.e., for periodic boundary conditions applied to the supercell). The change of parameter δ, determining the selection of the unit cell in the 1D MC on the right side of the interface, does not influence on the band structure but affect on the geometry of the interface between two 1D MCs. Therefore, by changing δ, we influence on the interface modes' frequency without perturbing the band structure. Results are presented in Fig. 3d. Gray strips indicate the frequency ranges where a continuum of states is observed, while white regions represent common frequency gaps. Due to narrow gaps, we broke the frequency axis to extend region of band gaps. During the evolution of δ, the values: $\delta = \delta_1 = 0.15$, $\delta = \delta_2 = 0.65$, correspond to the scenario, when right 1D MC is build of centrosymmetric unit cell (see inset below Fig. 1b).

In the common frequency gaps, we find the pairs of interface modes localized on complementary interfaces between both 1D MCs. By blue color are marked states occupying central interface and by red color are marked states originating from periodic boundary conditions. For the centrosymmetric cases: $\delta = \delta_1, \delta_2$ (marked by vertical gray lines), both interfaces are equivalent, and the interface states are degenerated and localized on both interfaces at once. By changing the δ we can tune the frequency of interface modes and traverse the whole range of the frequency gap. For the whole range of $\delta = [0, 1)$ (note that $\delta = 0$ is equivalent to $\delta = 1$) the interface mode traverse the gap even few time, depending on the number of the decaying oscillation of Bloch function in the unit cell. These numbers increases for successive gaps.

It is worth noting that by the gradual changes of δ, we are continuously transiting between two different selection of centrosymmetric unit cell for the 1D MC on the right side of the interface (corresponding to δ_1 and δ_2). Such change will result in the flipping of the Zak phase for each band ($0 \leftrightarrow \pi$) and the negation of logarithmic derivative of Bloch function in every second gap, i.e., for the gaps opened at the edges of 1st BZ. This effect allows relating the (non)existence of interface modes for the cases: $\delta = \delta_1$ and $\delta = \delta_2$[6,8] (see Supplementary Information, Section 2). The gap around 7.5 GHz (presented in Fig. 3d) is opened at edge of the 1st BZ (between the bands $n = 1$ and $n = 2$), so the interface modes can exist either for $\delta = \delta_1$ or $\delta = \delta_2$—we observe here only for $\delta = \delta_2$.
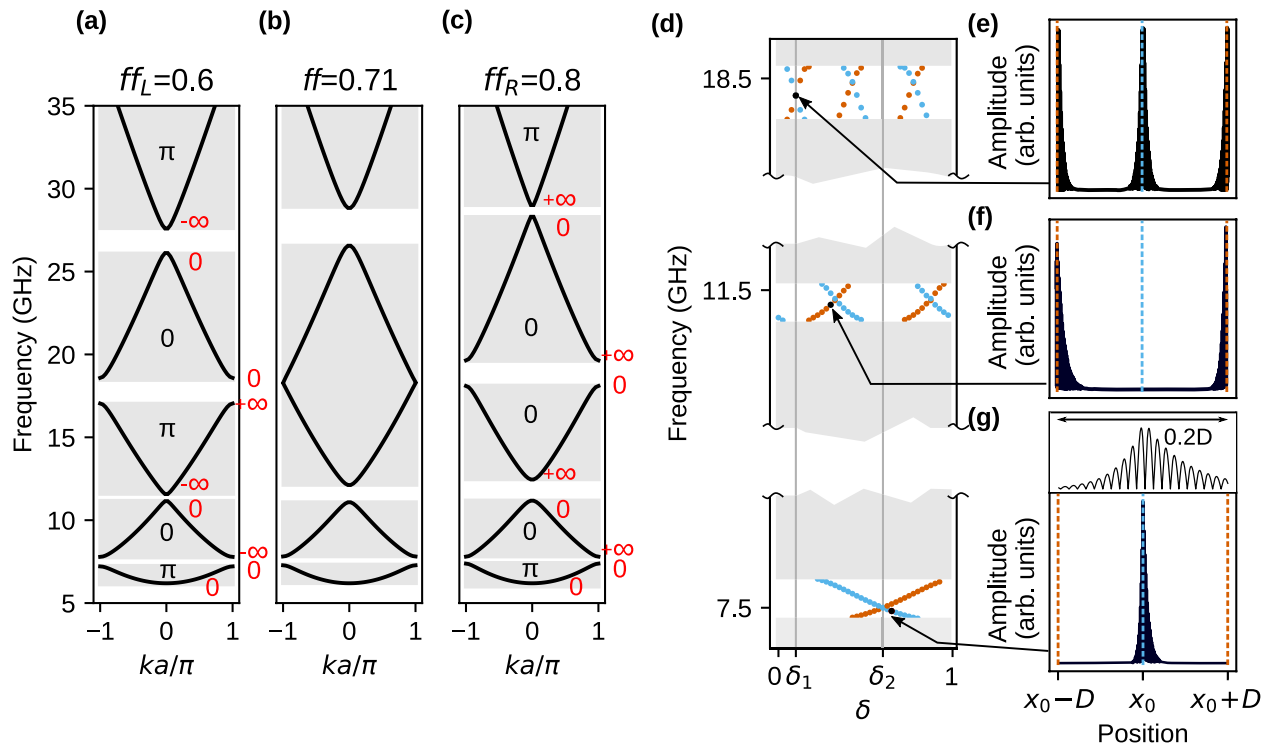
Figure 4. (**a**–**c**) Closing and reopening of the frequency gap (above the 1st band, at the edge of 1st Brillouin zone: $k = \pm\pi/a$) with the changes of filling fraction ff for exchange waves. The successive dispersion relations were plotted when the gap is (**a**) opened, $ff_L = 0.6$, (**b**) just closed, $ff = 0.71$, and (**c**) opened again, $ff_R = 0.8$. The values 0 and π are the Zak phases of the bands, 0 and ∞ (red color) stand for logarithmic derivative on the edges of band gaps. The values of Zak phases and logarithmic derivatives were determined for the case $\delta = \delta_1$ (i.e., for Co strip in the center of the unit cell). The SW interface modes localized on the interface of two MCs of $ff_L = 0.6$ and $ff_R = 0.8$. (**d**) The SW spectrum in the function of the surface parameter δ, defining the selection of the unit cells for 1D MC on the right. (**e**–**g**) The profiles of the SW interface modes in the gaps above 1st, 2nd and 3rd bands. We use the same conventions to mark the frequencies and localization of the SW interface modes as in Fig. 3e, f. Inset above (**g**) presents a close-up of the SW profile near the interface. It can be seen that despite the fact of decaying, the character of the mode is oscillating.

Whereas, the gap just above 11 GHz (Fig. 3d) is opened at the center of the 1st BZ (between the bands $n = 2$ and $n = 3$), which means that the existence conditions of interface modes are the same in both cases ($\delta = \delta_1, \delta = \delta_2$)—here we observe that they exist for both selections of centrosymmetric unit cell.

Interface modes for $ff_L = 0.6$ and $ff_R = 0.8$. The interface modes can also be found when we select different values of filling fractions for 1D MCs on the left and right side of the interface: $ff_L = 0.6$ and $ff_R = 0.8$ (Fig. 4a and c, respectively). For the intermediate value of the filling fraction $ff = 0.71$ (Fig. 4b), we observe the crossing of the gap's edges between third ($n = 3$) and forth ($n = 4$) band—see Fig. 2. The crossing of the bands allows matching the signs of the logarithmic derivatives in the third gap on both sides of the interface between two MCs (see also Supplementary Information, Section 2). However in Fig. 4c we can notice that Zak phase of third ($n = 3$) and forth ($n = 4$) band is 0. The reason for this is the additional swap of the Zak phase between the fourth and fifth band gap that is visible in Fig. 2. Regarding the Eq. (5), the sign of the logarithmic derivative is determined by the Zak phases of all bands below it, so the Zak phase of the band over the gap is irrelevant. The values of the logarithmic derivative at the edges of the gaps and the Zak phases superimposed on Fig. 4a–c was determined for centrosymmetric unit cell, i.e., for $\delta = \delta_1$—see also Fig. 2 in Supplementary Information, where the Zak phase was determined from the profiles of the Bloch functions at the edges of the bands.

The results of the SW spectra calculations ($k = 0$) of supercell with two jointed 1D MCs for $ff_L = 0.6$ and $ff_R = 0.8$ are presented in Fig. 4d–g. Figure 4d shows the SW spectra in the function of δ. In the considered frequency range, we can see three band gaps between the bands $n = 1, 2, 3, 4$. The interface states traverse between the edges of gaps, and the number of times increase with the number of band gaps. Similarly to the previous case ($ff_L = 0.4$, $ff_R = 0.7$), the interface modes appear in pairs and are localized in the middle of the supercell (Fig. 4g), at the edge of supercell (Fig. 4f) or at both locations (Fig. 4e)—due to degeneracy. The spatial oscillation of the interface modes are not visible because of the large number unit cells of each 1D MC ($N = 100$) within the supercell. The inset in top part of Fig. 4g shows the zoomed profile of interface mode in the vicinity of the interface. The modes has one oscillations per unit cell, therefore logarithmic derivative flips its sign once. As a results, this mode traverses once across the gap in the whole range of δ.
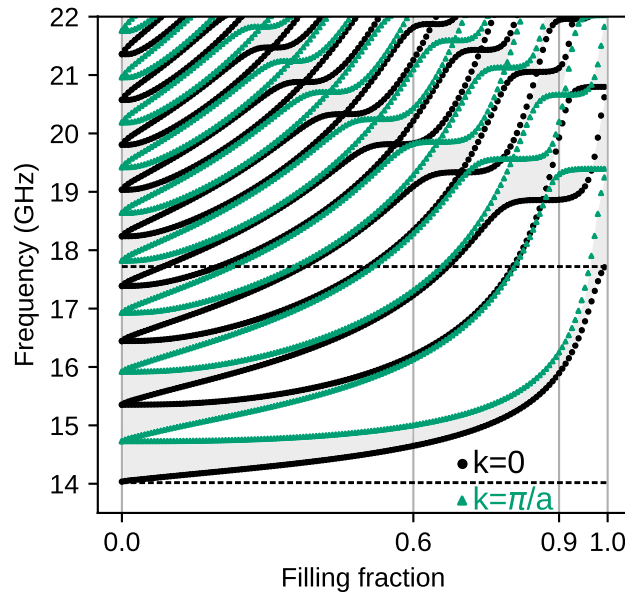
Figure 5. The evolution of dipolar-exchange SW spectra in dependence on the bulk parameter: filling fraction ff ($a = 1000$ nm). The vertical lines at $ff = 0.6, 0.9$ denote the pair of 1D MCs, that were interfaced. We used the same convention to mark frequency bands, gaps and their edges as in Fig. 2. The higher (lower) horizontal dashed line marks the FMR frequency for uniform Co (Py) layer.

We can analyze the existence of interface modes for two centrosymmetric cases $\delta = \delta_1$ and $\delta = \delta_2$ in similar way as for the structure $ff_L = 0.4$ and $ff_R = 0.7$. The gaps around 7.5 and 18.5 GHz open at the edge of the 1st BZ, therefore the interface state can be observed only for one selection of centrosymmetric unit cell. For the gap opened around 11.5 GHz, the absence of interface modes for $\delta = \delta_1$ implies the nonexistence of these states at $\delta = \delta_2$.

Dipolar-exchange spin waves. Let us now present the results for the system with included dipolar interactions. To observe the impact of dipolar interactions, we expanded the sizes of the system. The lattice constant is now larger by one order of magnitude: $a = 1000$ nm, referring to discussed case with exchange waves. Like in the previous section, we start from the analysis of SW spectra. Its dependence on the filling fraction ff is presented in Fig. 5. The first observation is that the fundamental mode is sensitive to magnetic parameters, contrary to spectrum with active only exchange interactions. The bottom of the 1st band ($k = 0$) is strongly dependent on ff. Starting from $ff = 0$, the frequency slowly increases from 14 GHz, while around $ff = 0.8$ it rises quickly, reaching ultimately about 17.5 GHz for $ff = 1$. The frequencies of the lowest SW modes (for $k = 0$) are just the frequencies of the ferromagnetic resonance (FMR), which is expressed as $f = \frac{|\gamma|\mu_0}{2\pi}\sqrt{H_0(H_0 + M_S)}$ for homogeneous layer of Py ($ff = 0$) or Co ($ff = 1$), differing significantly in saturation magnetization $M_{S,Py} < M_{S,Co}$. Therefore, the FMR frequency increases with the increase of filling fraction: $0 < ff < 1$. We marked the FMR frequencies of uniform Py and Co films by dashed lines.

The frequencies for other edges of the bands/gaps quickly increase with the ff too. However, their interweaving is not observed for low values of ff and low frequencies. It can be understood when we notice that the band crossing in 1D bi-component magnonic crystal requires the oscillatory solution in both components (strips, layers). In our system, the evanescent waves exist in Co strips for the frequencies below the FMR frequency of uniform Co. Additionally, due to confinement effect the frequencies of oscillatory modes in Co are increased for smaller ff where the Co strips are narrow. Therefore, to find the interface states, we selected a pair of MCs of relatively high filling fractions ff: 0.6|0.9 for which the edges of gaps can have different number of crossing points, that is related to different topological properties of their band structures.

The dispersion relations for these 1D MCs are presented in Fig. 6a, b. For reference, we showed the dispersion relations of the uniform film made of Co and Py in the range of $(-\pi/a, \pi/a)$. They are marked with dashed lines. Thanks to this comparison, we can attribute the first branch of MC in Fig. 6a as excitation in Py, while the fifth in Co. In Fig. 6b, the first branch of 1D MC is an excitation in Py, while the third one is an excitation in Co. The character of SW's profile is implicitly presented in Supplementary Information, Section 4. These bands are shifted up with respect to fundamental excitation in the uniform film due to the confinement and dipolar pinning in the strips[49]. The SW is forced to be quantized within the strip, and due to this, its frequency increase. For $ff = 0.9$ and the Py strip, this effect is the most significant because the Py strip is the narrowest—it has there only 100 nm. For $ff_R = 0.9$, two first bands have a minimum at the center of BZ, and a maximum at the edge of BZ. It violates the typical scenario when the maximum and minimum of two successive bands appear at the same position in BZ, i.e., the case when we observe only the direct gaps. This peculiarity of the system can be explained when we notice that the second band is not a result of folding the first band into the 1st BZ, but is related to the
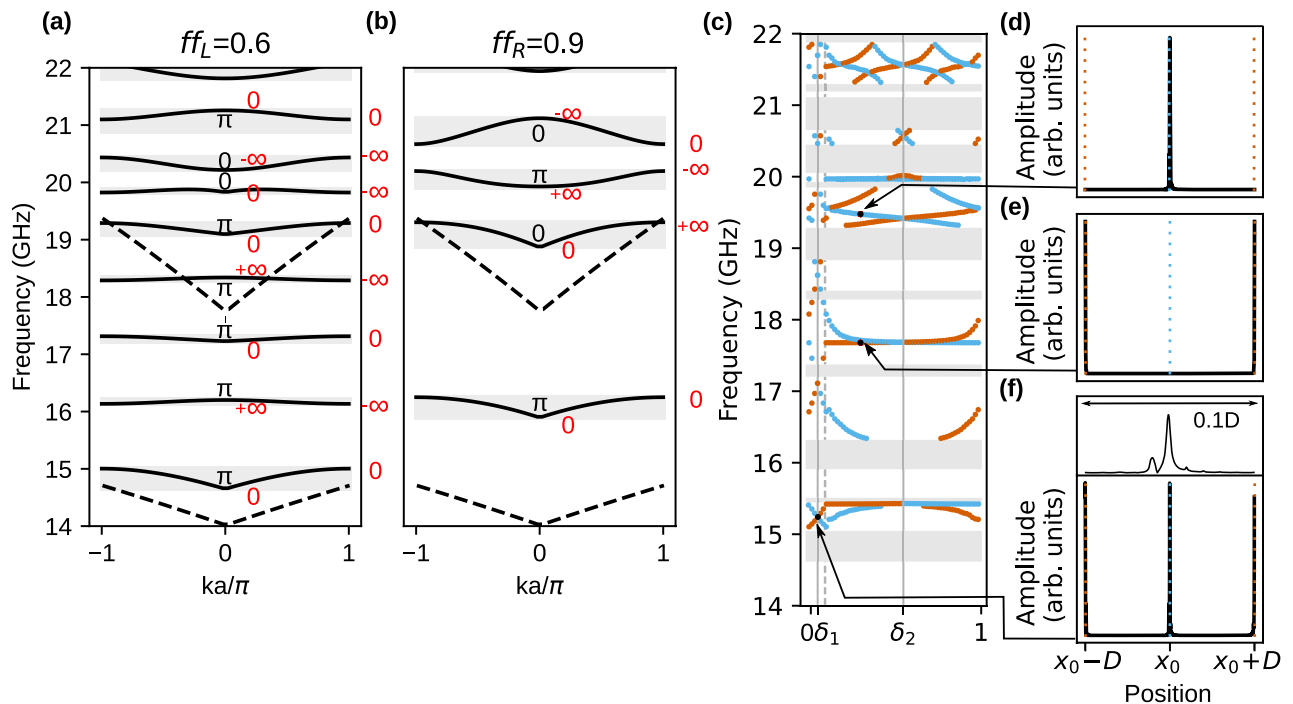
Figure 6. (**a**, **b**) The dipolar-exchange SW dispersion relations for two MCs which differ only in filing fractions: (**a**) $ff_L = 0.6$, (**b**) $ff_R = 0.9$. The spectrum for $ff = 0.9$ is shifted up in the frequency scale due to dipolar interaction, and the successive gaps in both spectra do not match each other. The forbidden ranges for interfaced MCs ($ff_L = 0.6$ and $ff_R = 0.9$) can originate from overlapping of various frequency gaps in both 1D MCs—see Fig. 5. The values: 0 and π are the Zak phases of the bands, whereas 0 and ∞ (red color) stand for logarithmic derivatives on the edges of bad gaps. Dashed lines represent dispersion relation for a uniform system made from Py (branch starts at 14GHz) and made from Co (branch starts at 17.5 GHz). (**c**) The dipolar-exchange SW interface modes localized on the interface of two 1D MCs of $ff_L = 0.6$ and $ff_R = 0.9$. The spectrum of SW interface modes is shown in dependence on the surface parameter δ. We use the same conventions to mark the frequencies and localization of the SW interface modes as in Fig. 3d. The gray dashed line denotes $\delta = 1 - ff$ where the Py|Co interface is on the left edge of the unit cell. (**d**–**f**) The profiles of the SW interface modes in common (from both 1D MCs) forbidden frequency ranges. The close-up at the $x = x_0$ is presented above (**f**). The SWs decay exponentially in Co strips and have one oscillation per Py strip.

lowest oscillatory solution in the Co strips. In the first band, we observe in Co the evanescent excitation forced by the magnetization dynamics in Py. This consideration is supported by spatial profiles of the modes presented in Supplementary Information, Section 4. It is worth noting that the lowest mode in Co can be also identified by the non-zero group velocity, characteristic of dipolar dynamical coupling in the limit $k \rightarrow 0$.

The spectrum of considered 1D MC's is very rich and is dramatically modified with the change of the filling fraction—the bands' positions and their separations (width of the gaps) vary significantly with ff. Unlike the system with exchange interaction only, the positions of corresponding band gaps (i.e., the band of the same index n) are different. For example, the first band gap for $ff_R = 0.9$ is located in the frequency range corresponding to second and third band gaps for $ff_L = 0.6$. The bands are relatively narrow which proves that we are operating in crossover dipolar-exchange regime. The flat dispersion branches in Fig. 6a–c means the low value of the group velocity for SW.

In Fig. 6a, b, we marked the Zak phases for centrosymmetric unit cells ($\delta = \delta_1$). The values were determined by the inspection of the profiles of the Bloch functions at the edges of the bands (see Fig. 2e, f in Supplementary Information). The sequences of Zak phases allows determining the sign of logarithmic derivatives of Bloch function, ρ, in frequency gaps for MCs at left and right side of the interface. The values of ρ at edges of bands are marked in Fig. 6a, b with red color.

The careful inspection of the sign of ρ in common frequency gaps of both MCs (marked as white areas in Fig. 6a, b) allows indicating three common gaps in which the signs of ρ are opposite: gap below 1st band, gap around 18.5 GHz and tiny gap, slightly above 21 GHz. In these gaps, we did not find numerically any interface modes: Figure 6c does not present solution at these frequencies for $\delta = \delta_1$. Concluding, analysis of logarithmic derivative for dipolar-exchange waves is also valid tool to describe the existence criteria for interface modes.

This system posses some peculiarities. Due to disturbing the typical sequence of dispersion branches, logarithmic derivative can take the same values on the edges of band gaps. For $ff_R = 0.9$ first band gap ρ is equal to 0 on both of the edges, and in second gap is equal to $-\infty$. We were also not able to plot the logarithmic derivatives of Bloch functions, as we did for exchange waves in Supplementary Information, Section 2. It is related to the

difficulties with the determination of the complex wavenumber in the indirect gaps, needed to be specified to run the PWM calculations.

For selected pair of the filling fractions ($ff_L = 0.6$, $ff_R = 0.9$) of two 1D MCs, we performed the numerical studies of the modes localized at interface between 1D MCs. Using the PWM and supercell approach, we calculated the frequencies and profiles of interface modes localized on two complementary interfaces. The frequencies were plotted in dependence on the parameter δ which describes the selection of the unit cell in the MC on the right side of the interface. Figure 6d presents the evolution of interface states in the function of δ. The first observation is that the dependencies of the frequencies of interface modes on the unit cell shift δ can change their slopes abruptly. This effect is related to the sensitivity of dipolar interaction on the interfaces. With an increasing value of δ, the narrow Py strip ($ff = 0.9$) moves into the center of the unit cell (see the inset below Fig. 1b for graphical illustration). Till the δ reach the value marked by the gray dashed line $\delta = 1 - ff$, the Py strip on the interface is widening. After that, the Co strip starts to be located on the interface, so the MC on the left starts to be interfaced with different material on the right side.

The another interesting finding is the absence of multiple traverses of the interface modes across the common gap for the swap of parameter δ, observed for small frequencies (below 19.5 GHz, where the modes start spatially oscillate in Co) and for the larger values of the δ ($1 - ff < \delta < 1$, where the left edge of the unit cell of the right MC appears in Co strip). In this range of the δ, the solution at the edge of unit cell (which is the right side on interface between 1D MCs, as well) cannot change the sign. It is because of the evanescent profile of the mode in Co. This excludes multiple flips of the sign of the mode at the interface while δ is changed.

Figure 6d–f shows the profile of the interface states for selected values of δ and frequency. They are strongly localized on the interface. Inset above (d) presents a close-up of the interface region. The oscillatory character is only in the Py strips, while in Co, the amplitude decay exponentially. The strong localization is a consequence of wide gaps in which the imaginary parts of wavevector (describing the exponential rate of localization) can reach large values.

Summary

We have presented a comprehensive study on the existence of interface SW states in 1D planar magnonic crystals, using a continuous model of magnetization dynamics for the exchange and dipolar-exchange spin waves.

We have related bulk parameter in magnonic crystal to the symmetry-related conditions of existence of interface states: (i) the concept of Zak phase, which is a topological characteristic of individual bands in the frequency spectrum was connected to (ii) the logarithmic derivative of the Bloch function on both sides of the interface, expressing the boundary conditions for interface modes in the band gaps. We have also performed numerical results that allowed us to consider the behavior of the interface modes for non-centrosymmetric unit cells. We have shown that this degree of freedom can be used to induce or vanish the interface state in desired band gap.

Full analogy to the already investigated electronic and photonic systems is observed in the magnonic system where the dipolar interactions are neglected. For the dipolar-exchange waves, however, the analysis becomes more complex. We have observed new effects specific to dipolar interaction: (i) rarer crossings of band gap edges—the band gaps do not close in a wide range of the filling fraction and the selection of pair of MCs with band structures supporting interface modes is challenging; (ii) in the lower-frequency range (i.e., in lower band gaps) the observed interface modes do not traverse the band gap edges with shifting MC unit cell. Nevertheless, we have found numerous interface modes, and their existence (for centrosymmetric unit cell) was determined from the symmetry criterion of the Bloch function on the band edges.

Data availability

The datasets used and analyzed during the current study available from the corresponding author on reasonable request.

References

1. Berry, M. V. Quantal phase factors accompanying adiabatic changes. *Proc. R. Soc. Lond. A Math. Phys. Sci.* **392**, 45–57. https://doi.org/10.1098/rspa.1984.0023 (1984).
2. Chern, S.-S. Characteristic classes of Hermitian manifolds. *Ann. Math.* **47**, 85–121. https://doi.org/10.2307/1969037 (1946).
3. Kane, C. Topological band theory and the $\mathbb{Z}_2$ invariant. In *Topological Insulators Contemporary Concepts of Condensed Matter Science*, Vol. 6 (eds Franz, M. & Molenkamp, L.) 3–34 (Elsevier, 2013).
4. Silveirinha, M. G. Chern invariants for continuous media. *Phys. Rev. B* **92**, 125153. https://doi.org/10.1103/PhysRevB.92.125153 (2015).
5. Zak, J. Band center–a conserved quantity in solids. *Phys. Rev. Lett.* **48**, 359–362. https://doi.org/10.1103/PhysRevLett.48.359 (1982).
6. Zak, J. B̀errys phase for energy bands in solids. *Phys. Rev. Lett.* **62**, 2747–2750. https://doi.org/10.1103/PhysRevLett.62.2747 (1989).
7. Atala, M. *et al.* Direct measurement of the Zak phase in topological Bloch bands. *Nat. Phys.* **9**, 795–800. https://doi.org/10.1038/nphys2790 (2013).
8. Zak, J. Symmetry criterion for surface states in solids. *Phys. Rev. B* **32**, 2218–2226. https://doi.org/10.1103/PhysRevB.32.2218 (1985).
9. Rhim, J.-W., Behrends, J. & Bardarson, J. H. Bulk-boundary correspondence from the intercellular Zak phase. *Phys. Rev. B* **95**, 035421. https://doi.org/10.1103/PhysRevB.95.035421 (2017).
10. Kohn, W. Analytic properties of Bloch waves and Wannier functions. *Phys. Rev.* **115**, 809–821. https://doi.org/10.1103/PhysRev.115.809 (1959).
11. Wang, H.-X., Guo, G.-Y. & Jiang, J.-H. Band topology in classical waves: Wilson-loop approach to topological numbers and fragile topology. *New J. Phys.* **21**, 093029. https://doi.org/10.1088/1367-2630/ab3f71 (2019).

12. Xiao, M., Zhang, Z. Q. & Chan, C. T. Surface impedance and bulk band geometric phases in one-dimensional systems. *Phys. Rev. X* **4**, 021017. https://doi.org/10.1103/PhysRevX.4.021017 (2014).

13. Nakata, Y., Ito, Y., Nakamura, Y. & Shindou, R. Topological boundary modes from translational deformations. *Phys. Rev. Lett.* **124**, 073901. https://doi.org/10.1103/PhysRevLett.124.073901 (2020).

14. Chen, W.-J. *et al.* Experimental realization of photonic topological insulator in a uniaxial metacrystal waveguide. *Nat. Commun.* **5**, 5782. https://doi.org/10.1038/ncomms6782 (2014).

15. Wang, L., Cai, W., Bie, M., Zhang, X. & Xu, J. Zak phase and topological plasmonic Tamm states in one-dimensional plasmonic crystals. *Opt. Express* **26**, 28963–28975. https://doi.org/10.1364/OE.26.028963 (2018).

16. Li, Z.-W., Fang, X.-S., Liang, B., Li, Y. & Cheng, J.-C. Topological interface states in the low-frequency band gap of one-dimensional phononic crystals. *Phys. Rev. Appl.* **14**, 054028. https://doi.org/10.1103/PhysRevApplied.14.054028 (2020).

17. Rychły, J., Kłos, J. W., Mruczkiewicz, M. & Krawczyk, M. Spin waves in one-dimensional bicomponent magnonic quasicrystals. *Phys. Rev. B* **92**, 054414. https://doi.org/10.1103/PhysRevB.92.054414 (2015).

18. Kruglyak, V. V., Demokritov, S. O. & Grundler, D. Magnonics. *J. Phys. D Appl. Phys.* **43**, 264001. https://doi.org/10.1088/0022-3727/43/26/264001 (2010).

19. Krawczyk, M. & Grundler, D. Review and prospects of magnonic crystals and devices with reprogrammable band structure. *J. Phys. Condens. Matter* **26**, 123202. https://doi.org/10.1088/0953-8984/26/12/123202 (2014).

20. Kłos, J. W. *et al.* Magnonics and confinement of light in Photonic–Magnonic crystals. In *Optomagnonic Structures: Novel Architectures for Simultaneous Control of Light and Spin Waves* 79–134 (World Scientific, Singapore, 2021).

21. Owerre, S. A. Floquet topological magnons. *J. Phys. Commun.* **1**, 021002. https://doi.org/10.1088/2399-6528/aa8843 (2017).

22. Pershoguba, S. S. *et al.* Dirac magnons in honeycomb ferromagnets. *Phys. Rev. X* **8**, 011010. https://doi.org/10.1103/PhysRevX.8.011010 (2018).

23. Mook, A., Henk, J. & Mertig, I. Edge states in topological magnon insulators. *Phys. Rev. B* **90**, 024412. https://doi.org/10.1103/PhysRevB.90.024412 (2014).

24. Shindou, R., Matsumoto, R., Murakami, S. & Ohe, J.-I. Topological chiral magnonic edge mode in a magnonic crystal. *Phys. Rev. B* **87**, 174427. https://doi.org/10.1103/PhysRevB.87.174427 (2013).

25. Mohseni, M. *et al.* Backscattering immunity of dipole-exchange magnetostatic surface spin waves. *Phys. Rev. Lett.* **122**, 197201. https://doi.org/10.1103/PhysRevLett.122.197201 (2019).

26. Yamamoto, K. *et al.* Topological characterization of classical waves: The topological origin of magnetostatic surface spin waves. *Phys. Rev. Lett.* **122**, 217201. https://doi.org/10.1103/PhysRevLett.122.217201 (2019).

27. Liu, J., Wang, L. & Shen, K. Dipolar spin waves in uniaxial easy-axis antiferromagnets: A natural topological nodal-line semimetal. *Phys. Rev. Res.* **2**, 023282. https://doi.org/10.1103/PhysRevResearch.2.023282 (2020).

28. Kruglyak, V. V., Sokolovskii, M. L., Tkachenko, V. S. & Kuchko, A. N. Spin-wave spectrum of a magnonic crystal with an isolated defect. *J. Appl. Phys* **99**, 08C906. https://doi.org/10.1063/1.2164419 (2006).

29. Kłos, J. W. & Tkachenko, V. S. Symmetry-related criteria for the occurrence of defect states in magnonic superlattices. *J. Appl. Phys.* **113**, 133907. https://doi.org/10.1063/1.4798607 (2013).

30. Lisenkov, I. *et al.* Spin-wave edge modes in finite arrays of dipolarly coupled magnetic nanopillars. *Phys. Rev. B* **90**, 104417. https://doi.org/10.1103/PhysRevB.90.104417 (2014).

31. Rychły, J. & Kłos, J. W. Spin wave surface states in 1d planar magnonic crystals. *J. Phys. D Appl. Phys.* **50**, 164004. https://doi.org/10.1088/1361-6463/aa5ae1 (2017).

32. Gallardo, R. A. *et al.* Symmetry and localization properties of defect modes in magnonic superlattices. *Phys. Rev. B* **97**, 174404. https://doi.org/10.1103/PhysRevB.97.174404 (2018).

33. Osokin, S., Safin, A., Barabanenkov, Y. & Nikitov, S. Spin waves in finite chain of dipolarly coupled ferromagnetic pillars. *J. Magn. Magn. Mater.* **465**, 519–523. https://doi.org/10.1016/j.jmmm.2018.06.041 (2018).

34. Zhou, J. *et al.* Precessional dynamics of geometrically scaled magnetostatic spin waves in two-dimensional magnonic fractals. *Phys. Rev. B* **105**, 174415. https://doi.org/10.1103/PhysRevB.105.174415 (2022).

35. Wang, Z. K. *et al.* Observation of frequency band gaps in a one-dimensional nanostructured magnonic crystal. *Appl. Phys. Lett.* **94**, 083112. https://doi.org/10.1063/1.3089839 (2009).

36. Tacchi, S. *et al.* Forbidden band gaps in the spin-wave spectrum of a two-dimensional bicomponent magnonic crystal. *Phys. Rev. Lett.* **109**, 137202. https://doi.org/10.1103/PhysRevLett.109.137202 (2012).

37. Choudhury, S. *et al.* Shape- and interface-induced control of spin dynamics of two-dimensional bicomponent magnonic crystals. *ACS Appl. Mater. Interfaces* **8**, 18339–18346. https://doi.org/10.1021/acsami.6b04011 (2016).

38. Wawro, A. *et al.* Magnetic properties of coupled Co/Mo/Co structures tailored by ion irradiation. *Phys. Rev. Appl.* **9**, 014029. https://doi.org/10.1103/PhysRevApplied.9.014029 (2018).

39. Frackowiak, L. *et al.* Magnetic domains without domain walls: A unique effect of he$^+$ ion bombardment in ferrimagnetic Tb/Co films. *Phys. Rev. Lett.* **124**, 047203. https://doi.org/10.1103/PhysRevLett.124.047203 (2020).

40. Chang, C. L. *et al.* Driving magnetization dynamics in an on-demand magnonic crystal via the magnetoelastic interactions. *Phys. Rev. Appl.* **10**, 064051. https://doi.org/10.1103/PhysRevApplied.10.064051 (2018).

41. Topp, J., Heitmann, D., Kostylev, M. P. & Grundler, D. Making a reconfigurable artificial crystal by ordering bistable magnetic nanowires. *Phys. Rev. Lett.* **104**, 207205. https://doi.org/10.1103/PhysRevLett.104.207205 (2010).

42. Mamica, S., Krawczyk, M. & Grundler, D. Nonuniform spin-wave softening in two-dimensional magnonic crystals as a tool for opening omnidirectional magnonic band gaps. *Phys. Rev. Appl.* **11**, 054011. https://doi.org/10.1103/PhysRevApplied.11.054011 (2019).

43. Mruczkiewicz, M. & Krawczyk, M. Nonreciprocal dispersion of spin waves in ferromagnetic thin films covered with a finite-conductivity metal. *J. Appl. Phys.* **115**, 113909. https://doi.org/10.1063/1.4868905 (2014).

44. Bessonov, V. D. *et al.* Magnonic band gaps in yig-based one-dimensional magnonic crystals: An array of grooves versus an array of metallic stripes. *Phys. Rev. B* **91**, 104421. https://doi.org/10.1103/PhysRevB.91.104421 (2015).

45. Langer, M. *et al.* Spin-wave modes in transition from a thin film to a full magnonic crystal. *Phys. Rev. B* **99**, 024426. https://doi.org/10.1103/PhysRevB.99.024426 (2019).

46. Teschl, G. *Ordinary Differential Equations and Dynamical Systems* (The American Mathematical Society, Rhode Island, 2012).

47. Krawczyk, M., Sokolovskyy, M. L., Kłos, J. W. & Mamica, S. On the formulation of the exchange field in the Landau-Lifshitz equation for spin-wave calculation in magnonic crystals. *Adv. Condens. Matter Phys.* **2012**, 14. https://doi.org/10.1155/2012/764783 (2012).

48. Rychły, J., Mieszczak, S. & Kłos, J. Spin waves in planar quasicrystal of penrose tiling. *J. Magn. Magn. Mater.* **450**, 18–23. https://doi.org/10.1016/j.jmmm.2017.03.029 (2018).

49. Centała, G. *et al.* Influence of nonmagnetic dielectric spacers on the spin-wave response of one-dimensional planar magnonic crystals. *Phys. Rev. B* **100**, 224428. https://doi.org/10.1103/PhysRevB.100.224428 (2019).

Acknowledgements

Author contributions

J.W.K. brought the idea to consider interface states in the joint two 1D magnonic crystals, S.M. did numerical calculations, S.M. and J.W.K. analyzed results and wrote manuscript.

Competing interests

The authors declare no competing interests.

Additional information

Supplementary Information The online version contains supplementary material available at https://doi.org/10.1038/s41598-022-15328-x.

Correspondence and requests for materials should be addressed to S.M.

Reprints and permissions information is available at www.nature.com/reprints.

Publisher's note Springer Nature remains neutral with regard to jurisdictional claims in published maps and institutional affiliations.